AGU ADVANCING EARTH AND SPACE SCIENCE

Geophysical Research Letters

RESEARCH LETTER
10.1029/2021GL097493

Tsunamigenic Potential of an Incipient Submarine Landslide in the Tiran Straits

Sam J. Purkis[1,2], Steven N. Ward[3], Hannah Shernisky[1], Giovanni Chimienti[4], Arash Sharifi[1,5], Fabio Marchese[6], Francesca Benzoni[6], Mattie Rodrigue[7], Maureen E. Raymo[8], and Ameer Abdulla[1,9]

[1]CSL – Center for Carbonate Research, Department of Marine Geosciences, Rosenstiel School of Marine and Atmospheric Science, University of Miami, Miami, FL, USA, [2]Khaled Bin Sultan Living Oceans Foundation, Annapolis, MD, USA, [3]Institue of Geophysics and Planetary Physics, University of California Santa Cruz, Santa Cruz, CA, USA, [4]Department of Biology and CoNISMA LRU, University of Bari Aldo Moro, Bari, Italy, [5]Beta Analytic Inc., Miami, FL, USA, [6]King Abdullah University of Science and Technology, Thuwal, Saudi Arabia, [7]OceanX, New York, NY, USA, [8]Lamont-Doherty Earth Observatory, Columbia University, Palisades, NY, USA, [9]NEOM, Riyadh, Saudi Arabia

Key Points:

- An incipient submarine landslide started in the Tiran Straits, stalled, but likely still generated a 10 m tsunami
- Tsunami produced by slides are fundamentally different from those formed by earthquake ruptures - even incipient landslides can spawn tsunami as tall as those from $M_w = 9$ earthquakes, at least locally
- Incipient failures also carry the dual threat of eventually sliding to completion, yielding still larger tsunami sometime in the future. This hazard is especially amplified in narrow basins like the Red Sea

Supporting Information:

Supporting Information may be found in the online version of this article.

Correspondence to:

S. J. Purkis,
spurkis@rsmas.miami.edu

Citation:

Purkis, S. J., Ward, S. N., Shernisky, H., Chimienti, G., Sharifi, A., Marchese, F., et al. (2022). Tsunamigenic potential of an incipient submarine landslide in the Tiran Straits. *Geophysical Research Letters*, *49*, e2021GL097493. https://doi.org/10.1029/2021GL097493

Received 14 DEC 2021
Accepted 24 JAN 2022

Author Contributions:

Conceptualization: Sam J. Purkis
Data curation: Sam J. Purkis, Giovanni Chimienti, Arash Sharifi
Formal analysis: Sam J. Purkis, Giovanni Chimienti, Arash Sharifi
Funding acquisition: Sam J. Purkis, Mattie Rodrigue, Ameer Abdulla
Investigation: Sam J. Purkis, Giovanni Chimienti, Fabio Marchese, Francesca Benzoni

Abstract The Red Sea is a maritime rift. Tsunamigenic submarine landslides are common in these deep, steep-sided, and seismically active basins. Because the rift is narrow, tsunami formed on one margin dissipate little before impacting the opposite side. Red Sea slope failures are therefore especially hazardous. We examine the tsunamigenic potential of an incipient landslide in the Tiran Straits that started, but then stopped after a short distance. Radiometric and biotic analyses fix the age of this landslide to within the last 500 years. Tsunami modeling of the incipient slide predicts ~10 m wave heights on the Egyptian coastline. Of present concern is that the slope will eventually slide to completion with even more hazardous results. Tsunami simulated for this future event are twice as large as that generated by the incipient slide, so the threat posed by a future slide is consequential. Sharm El Sheikh, an Egyptian resort town now lies in its path, as does "The Line," a vast Saudi infrastructure project. This study warns of credible tsunami risk in the rapidly urbanizing Tiran Straits.

Plain Language Summary We present the discovery of an incipient submarine landslide in the Tiran Straits. Our study reveals how even incipient submarine landslides can spawn tsunami as tall as those from $M_w = 9$ earthquakes, at least locally. Incipient failures also carry the dual threat of eventually sliding to completion, yielding still larger tsunami sometime in the future. Should this incipient slide complete, it will gravely threaten the rapidly urbanizing coastline of the Tiran Straits and adjacent Gulf of Aqaba.

1. Introduction

The Tiran Straits separate the Gulf of Aqaba from the Red Sea. Their tectonic configuration is characterized by the Dead Sea Transform (DST) fault system (Augustin et al., 2021; Ben-Avraham, 1985; Ben-Avraham et al., 1979; Garfunkel, 2014; Ribot et al., 2021; Figure 1). The Tiran Straits are seismically active (Figure 2a) and at risk of tsunami generated both by coseismic seabed deformation and submarine sliding of the thick seabed accumulations of aeolian dust, biogenic carbonates, and siliciclastic sediments deposited during episodic flashfloods from the numerous ephemeral rivers (wadis) distributed along the coasts (Katz et al., 2015). Much focus has been placed on the 1995 Nuweiba earthquake ($M_w = 7.1$) that occurred along the DST fault system (Abdel-Fattah et al., 1997; Baer et al., 1999; Klinger et al., 1999; Tibor et al., 2010), generating a modest tsunami (Frucht et al., 2019). The 1969 Shadwan earthquake ($M_w = 6.8$) was also likely tsunamigenic (Ben-Menahem, 1991). Evidence from Eilat alludes to a major tsunami dating to 2.3 ka BP (Goodman Tchernov et al., 2016; Shaked et al., 2004) and deposits on the Egyptian coast have been proposed as tsunamigenic (Salem, 2009), though their timing is equivocal.

By virtue of a pair of huge Saudi infrastructure projects, understanding tsunami risk in the Straits has gained urgency. Of these, the first is the King Salman Bridge which, if built, will span the Straits via Tiran Island, linking Egypt and Saudi Arabia. The second project is a smart city, "The Line," which has moved from the drawing board to construction in Saudi's Neom area, abutting the Straits. Among a raft of ambitious firsts, Neom, will become a global center for hydrogen production. Finally, the Egyptian resort town of Sharm El Sheikh sits on a promontory overlooking the Straits.

Methodology: Sam J. Purkis, Arash Sharifi
Project Administration: Fabio Marchese, Francesca Benzoni, Mattie Rodrigue
Resources: Hannah Shernisky
Supervision: Sam J. Purkis, Ameer Abdulla
Validation: Sam J. Purkis, Hannah Shernisky
Writing – original draft: Sam J. Purkis
Writing – review & editing: Sam J. Purkis, Maureen E. Raymo

This study builds on the discovery of a pronounced scarp on the eastern margin of the Straits during a submersible dive conducted as part of the 2020 OceanX-Neom expedition (Figures 1 and 2). Limited faunal colonization of the scarp, as compared to the adjacent seabed, suggests the feature to be geologically recent. Our aims are twofold. First, to decipher the provenance of this scarp. Second, to evaluate the tsunami hazard wrought by the processes that created it.

2. Materials and Methods

We compile a comprehensive geophysical data set spanning the northern Red Sea and Gulf of Aqaba. These data were acquired in 2020 with OceanX and full details are available in Supporting Information S1. Two cases of complete margin failure situate <5 km to the north of the incipient scarp (Figures 1 and 2). As developed in Supporting Information S1, both failures likely date to the Holocene, thereby confirming that this sector of the shelf is prone to collapse. Quantitative analysis of the biota colonizing the incipient scarp was accomplished by examining videos captured during submersible dives. These data were assembled to diagnose whether the incipient scarp was created by a single large event and to estimate the elapsed "time of exposure" since it formed. The specifics of these analyses are captured in Supporting Information S1. Timing of the incipient failure was constrained using ^{14}C and U-series dating of the coral framework and lithified (compacted and cemented) sediments which constitute the scarp face (Figure 3). Full details on sample preparation and radiometric dating are provided in Supporting Information S1.

Simulations of the incipient and full submarine landslides were accomplished using the Tsunami Squares method (Wang et al., 2015, 2019; Xiao et al., 2015). For these models, the map boundaries of landslide-source material follow the 6 km-long trace of the observed scarp at the top, and extend directly down slope to a water depth of 650 m (Figure 2b). The bottom of the slide mass is fixed by a curved and sloping basal surface. At the toe of the slide, the basal surface cuts the slope face obliquely. At the head of the slide, the basal surface becomes nearly vertical and intersects the observed scarp (Figure 4). The target depth to the basal surface was set to 50 m or 100 m. In all cases, the initial landslide-source area covered 4.70 km^2, but with source volumes of either 0.26 km^3 or 0.52 km^3. A more detailed description of the tsunami model setup is given in Supporting Information S1.

3. Results and Discussion

3.1. Physical Characteristics of the Scarp

The top of the scarp situates at 90 m water depth, within the mesophotic zone (Kahng et al., 2019). This feature is 6 km long and averages a height of 8 m. The slope on which the scarp is located drops away at an angle of >30° into the Tiran Deep to a water depth of 1,200 m. The base of the slope in this area is demarked by the sinistral strike-slip Tiran fault (Figure 2), emphasizing the potential for seismicity. The scarp breaks a gently sloped seabed colonized by a heterogeneous community of hermatypic stony-corals of the genus *Leptoseris*, whip-like black corals of the genus *Cirripathes*, and fan-like black corals tentatively assigned to the family Aphanipathidae, as well as a suite of octocorals including *Parisis* sp., *Acanthogorgia* sp., *Acanthomuricea* sp., *Keroeides* sp., *Acabaria* spp. (Figure S1 in Supporting Information S1). The scarp face, by contrast, is sparsely colonized by a low-diversity assemblage dominated by fan-like colonies of *Acanthogorgia* sp. and Aphanipathidae, with occasional small *Leptoseris* sp.

3.2. The Scarp Is an Incipient Slide, Not an Earthquake Fault

The scarp that we found could have been created in two ways. The first is by earthquake faulting. The second is by incipient (partial) margin failure, a submarine landslide. We consider the merits of both mechanisms, starting with faulting.

The geometry of the scarp could be compatible with the rupture of a SE-dipping reverse fault. Reverse faulting, however, is uncharacteristic of the Red Sea rift and, in particular, of the strike-slip displacement of the Tiran fault, which bounds the base of the slope on which the scarp situates (Figure 2). More reasonably, the scarp might be attributed to displacement along a NW-dipping normal fault that has experienced footwall uplift (Bosworth et al., 2017; Wawrzyniec et al., 2001; Yielding & Roberts, 1992). Normal faulting of this type serves to uplift Tiran Island, consistent with the discovery of a horst underlying the Straits (Mart et al., 2018).

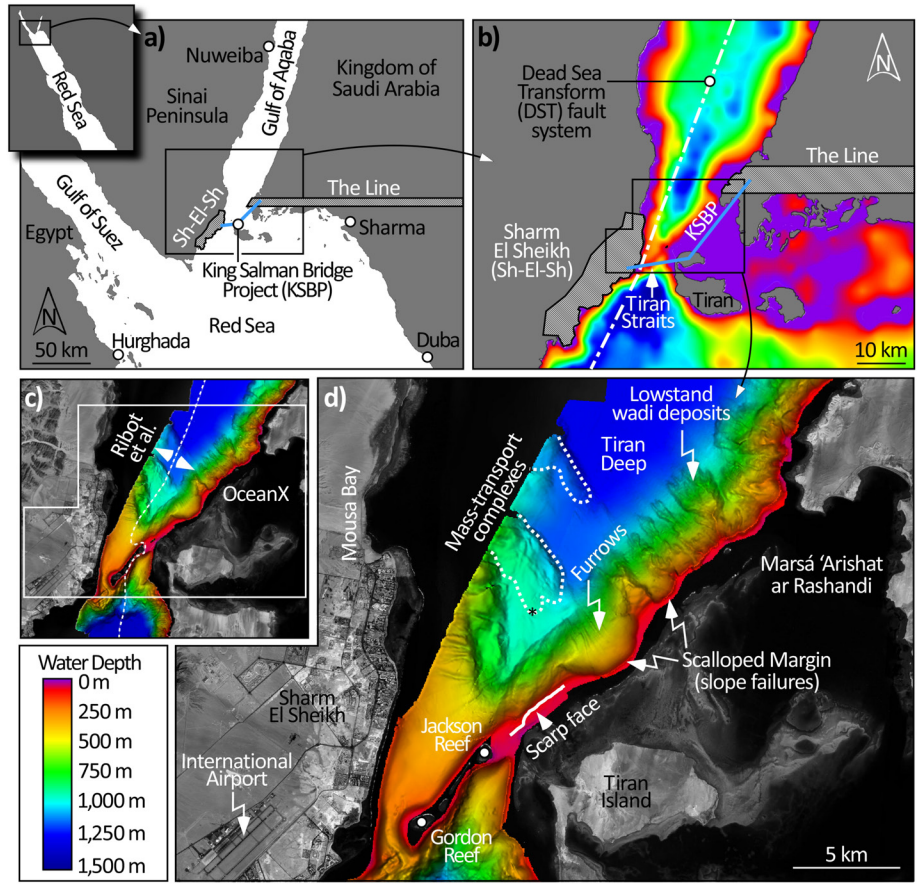

Figure 1. Location of the study area in the Tiran Straits, tectonic setting, and bathymetry: The strike-slip Dead Sea Transform (DST) fault system (*white dot-dash line* in b) runs along the axis of the Straits and is composed of several systematically offset, overlapping, left-lateral transform faults. Local infrastructure includes the Egyptian town of Sharm El Sheikh (approx. city limits, *hatched polygon* in a and b), and planned construction of "The Line," a 170 km-long east-west-trending city (*hatched rectangle* in b), and the King Salman Bridge Project which would straddle Tiran Island (*blue line* in a-b, position approximate). (c) Multibeam bathymetry created by merging data from Ribot et al. (2021), west of the *broken white line* in (c), with that acquired by OceanX (east of *broken white line*). (d) Enlarges the bathymetry offshore Sharm El Sheikh including the location of the scarp face and two instances of slope failure to the north of it, recognized by the paired occurrences of scallop "bite" marks in the eastern margin of the Straits with mass-transport complexes (delimited by *broken white lines*) lying outboard of them on the abyssal plain of the Tiran Deep. Submersible dive (*black asterisk*) on the southernmost complex confirmed abundant breccia blocks. Margin-perpendicular furrows are evident on areas of the slope that have failed, likely excavated by cascading density currents. To the northeast of the two paleo-slope failures, canyon heads at the shelf break have been fed by wadis during sea-level lowstands, delivering substantial deposits to the abyssal plain.

If a single event created the scarp, as the uniformly scant biotic colonization of its face intimates, ascribing its formation to one faulting episode flaunts a fundamental scaling law of earthquake rupture. Rupture area scales with average coseismic displacement according to a power law (Thingbaijam et al., 2017), dictating that displacements measured in meters associate with fault areas of thousands of square kilometers. If the scarp is indeed an earthquake rupture, to have an average displacement of 8 m, as measured in the field, that rupture should be associated with a fault area of ~10,000 sq. km. This is more than 3× the area of the entire Gulf of Aqaba and therefore untenable. Further, if the scarp indeed charts a normal fault, it would be at right angles to the faults mapped adjacent to Tiran Island (Goldberg & Beyth, 1991) which lie <1 km away (Figure 2a). An unlikely configuration and further evidence that the scarp is not from an earthquake rupture.

A more reasonable interpretation may be that the scarp scar resulted from an incipient submarine landslide that started but stopped after a short distance. This interpretation is supported by the fact that the margin situated just to the north of the scarp displays two characteristic scallop "bite" marks of catastrophic slope failure (Figures 1d and 2). Outboard of these scallops, features consistent with mass-transport complexes are visible in the

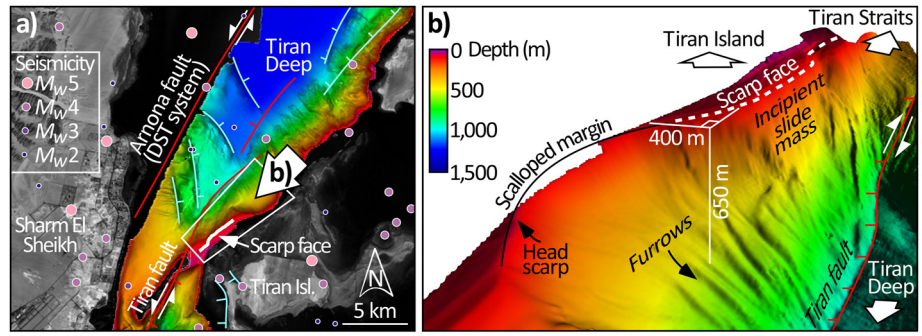

Figure 2. Seismotectonic setting of the Tiran Straits and southern Gulf of Aqaba: (a) Shows the main active faults in the vicinity of the Straits (modified from Goldberg & Beyth, 1991 and from Ribot et al., 2021) and $M_w \geq 2$ earthquakes for the period 1970–2021 (U.S. Geological Survey). Strike-slip faults are in *red*. Both the Tiran and Arnona faults are part of the strike-slip Dead Sea Transform (DST) fault system (Figure 1b). Normal faults are in *cyan*. The area in the white polygon is shown in three dimensions in (b). Here, vertical exaggeration is ×2.5 and the observer is looking from the northeast, along the Saudi margin of the Gulf of Aqaba, toward the Straits. The scarp face (*broken white line*) situates immediately adjacent to a scallop which demarks a previous margin failure. We interpret the slide mass from the incipient failure which generated the scarp to extend down-slope to a water depth of 650 m. The toe-of-slope beneath this mass is at 850 m depth and bounded by the Tiran fault.

multibeam data, where material shed from the failed margin has accumulated in the abyssal Tiran Deep. A submersible dive conducted on one complex (asterisk, Figure 1d) confirmed abundant slope-derived "mega" breccia blocks at 950 m depth. These observations imply that the margin where the scarp is located is prone to failure.

Examination of the multibeam data in a sequence-stratigraphic context allows the age of these previous failures to be estimated. Absent from both slides are the canyon heads and wadi deposits which characterize the rest of the shelf (Figure 1d), indicating that these failures occurred after the last lowstand, at 19 kyr BP. Meanwhile, the failure scars have been furrowed by cascading density currents (Figures 1d and 2b), which can only activate once the lagoon inboard of these slides, the Marsá 'Arīshat ar Rāshandī, was flooded by a sea-level highstand. These observations imply that the two margin failures date to the Holocene. Additional detail in Supporting Information S1.

3.3. The Incipient Slide Occurred Recently as a Single Event

The lack of diversity for the live coral inhabiting the scarp's face advocates that it is ecologically young. The scarp hosts only two dominant coral taxa whereas the surrounding seabed is colonized by > 10 taxa (Figures 3a–3c and Figure S1 in Supporting Information S1). Further, the coral community densities on the upper and lower scarp (defined as spanning water depths of 90–94 m and 94–98 m, respectively) are not statistically different ($p > 0.05$; Figure 3d), indicating that the scarp took shape rapidly by a single event.

To further constrain its timing of formation, seven rock samples were collected along a vertical transect of the scarp face, from its base to top (Figure 3). For full details, see Supporting Information S1. Of these, pristine coral skeletons could be unequivocally identified in three samples. Representative occurrences of the sediments, now lithified, that infilled the coral framework were targeted in the remaining four samples. ^{14}C dates for the sampled coral skeletons span 2,888–1,558 years. BP. Considering the young ecological age of the scarp established by its biota, which is lacking in number and variety of species, we assume that these coral skeletons comprise the original seabed which was broken by the slide. Hence, the slide must be younger than 1,558 years. BP. The lithified sediments that infilled the skeletons dated between 916 and 334 years. BP. For these, it is noteworthy that all the ages, bar the oldest (916 years), overlap at 2 sigma, emphasizing the possibility that the three ages spanning 536–334 years represent the spread produced by three measurements on material of the same age. This raises the prospect that the three youngest ages are dating an event at ~400–500 years. BP that removed any older matrix from the scarp face, as could plausibly have been affected by the pressure variations associated with the slide and likely tsunami. The voids created by this loss of matrix were subsequently infilled by younger material in the upper section of the scarp, which constitute the lithified sediments which we retrieved and dated. The survival of lithified sediment at greater depth (i.e., the 916 years date lower in the exposed section) might be explained by a

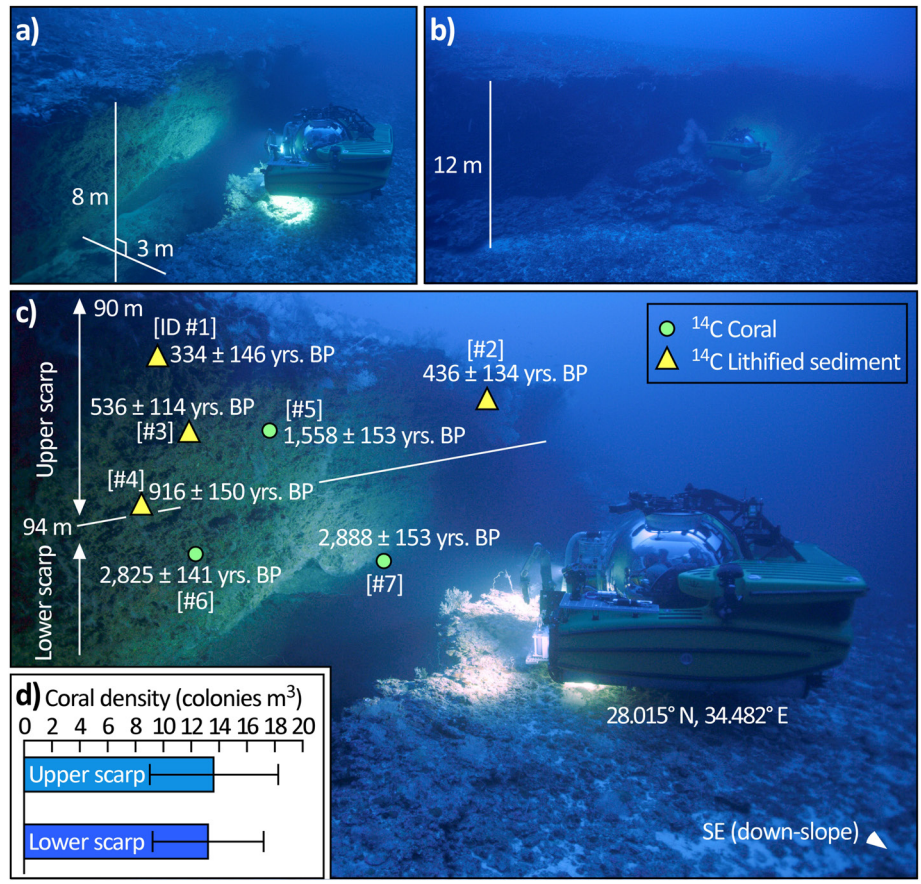

Figure 3. Radiocarbon dates and distribution of biota on the scarp face: (a and b) Representative photographs of the scarp. In both cases, the sub is facing southeast, into the scarp, toward Tiran Island. The abyssal depths of the Tiran Deep are therefore aft of the sub in these photographs. (a) Emphasizes that the scarp has both a vertical and lateral offset, which at this location measures 8 and 3 m, respectively. Panel (b) was acquired ~50 m back from the scarp and shows a location where the vertical offset attains 12 m, approaching the maximum vertical offset of 15 m encountered along the 6 km strike of the feature. (c) Either corals, or the (now lithified) sediments infilling their skeletons, were isolated from each rock sample extracted from the scarp and ^{14}C dated. Ages calibrated to calendar years BP (before present) with 2 sigma error reported. Sample IDs in square brackets reference Table S1 in Supporting Information S1. Corals range in age from 2,888 years to 1,558 years. BP. Lithified sediments are younger, ranging from 916 years to 334 years. BP. *White line* divides the scarp into upper (90–94 m water depth) and lower (94–98 m) units where mean density (±std) of coral colonies was quantified (d). The densities are not significantly different ($p > 0.05$), implying the scarp was created swiftly by a single event.

threshold in diagenesis causing older matrix sediment, deeper in the pre-landslide sequence, to be more resistant to excavation during the incipient landslide. Adopting this model, we interpret the meagre biotic diversity of the scarp and ^{14}C dating to imply that the incipient slide occurred within the last 500 years.

3.4. Even a Minor Slide Can Pose a Major Risk

We computed submarine landslides and parented tsunami using the Tsunami Squares method (Wang et al., 2015, 2019; Xiao et al., 2015; see Supporting Information S1). In the same vein as Sun and Leslie (2020), for the incipient slide, we assume that the entire slide mass, with the 50 m basal surface depth, began to move down slope briefly but then got hung up for some reason (Figure 4a). In 9 s, the incipient slide moved 35 m horizontally and 12 m vertically with a top speed of 7.3 m/s. This movement, hardly visible in Figure 4a, would have been enough to pull away down-slope material from the near-vertical basal surface at the slide head and create the scale of the observed scarp (Figure 3). The horizontal profile in Figure 4a plots the change in seafloor topography resulting from this slide. The sharp face of the newly formed head scarp (~10 m high) shows clearly there, as does the broader-scale uplift at the slide toe. Even though the incipient slide moved downslope just

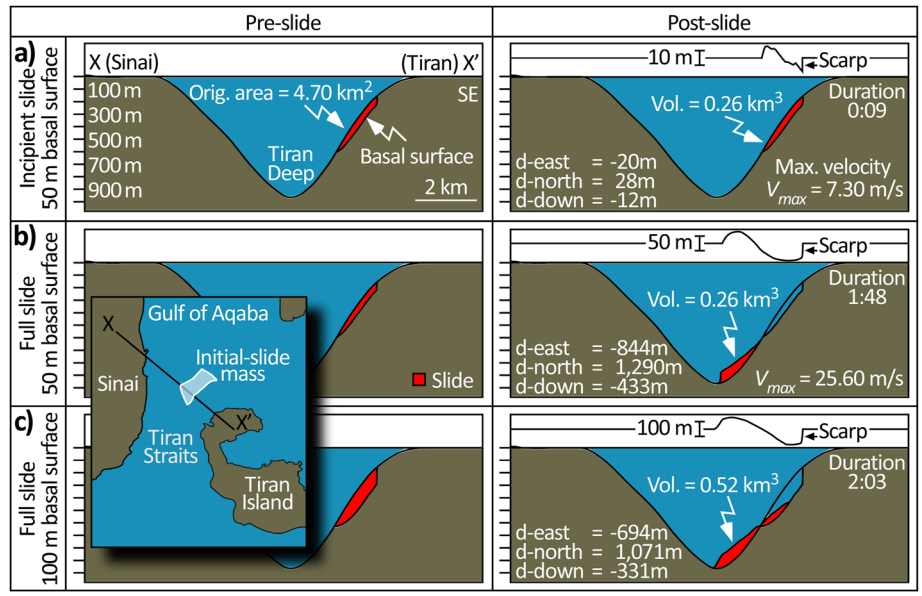

Figure 4. Setup of landslide simulations: Inset shows plan-view of the initial-slide mass (*white polygon*) and transect X to X′ spanning the Tiran Straits along which the cross sections of the three model configurations are developed. (a) Incipient slide with 50 m basal surface, (b) full slide with 50 m basal surface, and (c) full slide with a 100 m basal surface. In the pre-slide configurations, the top of the slide situates at 90 m water depth, the bottom at 650 m, and plan-view area is 4.70 km^2. The post-slide configuration shows the distance moved by the slide in x-y-z space (d-east, d-north, and d-down, respectively), the volume of the slide (Vol.), the maximum velocity reached (V_{max}), and duration of the slide. Horizontal profiles at top of the three post-slide panels trace the difference between post- and pre-slide topography of the seabed. Negative deviation of trace indicates a drop in seabed elevation (erosion). Positive deviation depicts a rise (deposition).

30 m, its tsunami was consequential. A 6 m-high wave impacted Sharm El Sheikh after 1 min and 30 s (T = 1:30; Figure 5a). 10 m waves reached Mousa Bay by T = 2:50 (Figure 5b) and similarly sized waves beached on the Saudi coast by T = 4:20 (Figure 5c).

Beyond retro-casting the tsunami from the incipient slide, we also forecast tsunami from two future scenarios where the incipient landslide runs to completion in a manner comparable to the styles of paleo-slides that we see just to the north. In these simulations, slide material moved down-slope for over 2 min, translating about 2,000 m horizontally and 300–400 m vertically. The only difference between these two cases is the depth to basal surface, 50 m in Figure 4b and 100 m in Figure 4c. Mass transport is now sufficient to expose the basal surfaces and create huge head scarps 50 and 100 m high. We feel that 50–100 m basal surface depths bracket the likely scale of landslide behaviors here, in line with analogous studies (Schnyder et al., 2016; Sun & Leslie, 2020).

Both cases evolve similarly with the first impacts at Sharm by T = 1:30. The simulation predicts wave heights at the coast of 21 and 35 m for the 50 m and 100-m-thick slides (Figures 5d–5f and 5g–5i). By T = 2:50, Mousa Bay experiences 30 and 45 m waves, for the two cases. By this time, waves have propagated ∼1 km inboard of Sharm's coastline. Saudi is again impacted at T = 4:20. Maximum wave heights taper down here but remain substantial (10 m at Ras Gasabah for the best-case scenario, 15 m for the worst case). We project comparably sized waves to enter the Marsá ʻArīshat ar Rāshandī at this time (location, see Figure 1d).

Conspicuous in all simulations is how the bathymetry of the Straits confines and directs the tsunami. The wide and deep water to the north allows the wavefront to progress unhindered up the Gulf of Aqaba. To the south, the narrow and shallow Straits restrict wave entry into the Red Sea.

One surprising result of the simulations is that the wave generated by the incipient slide, that lasted merely seconds and covered only 30 m, is just 2.5× smaller than the wave generated by the slide going to completion in 2 min and covering 2 km. So, increasing slip distance and duration by one order of magnitude only serves to double wave height. The incipient slide generates such a large wave relative to that of the full slide because most of the tsunami is generated at the beginning of the landslide, in shallow water. As emphasized in the animations (Supporting Information S1), whereas the complete margin collapse plays out over a duration of 2 min, the first

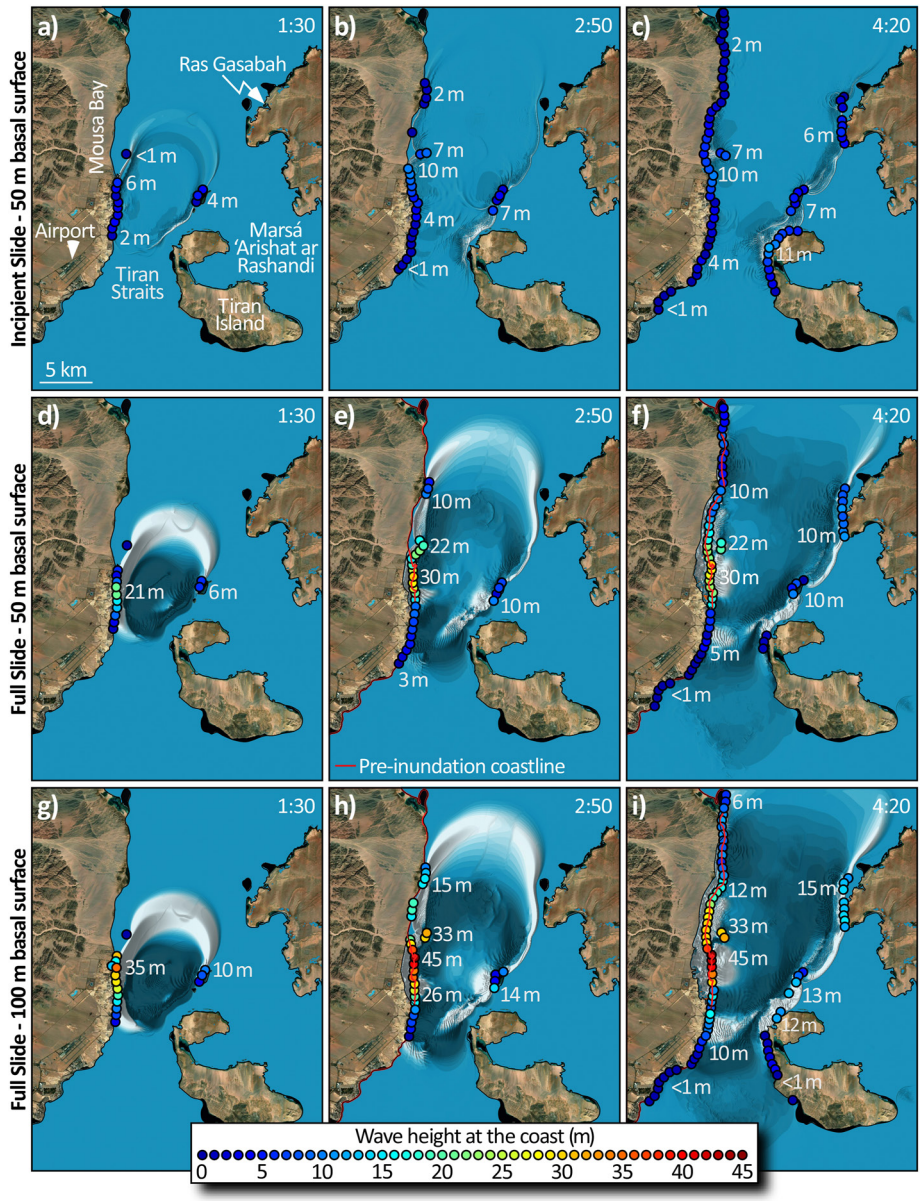

Figure 5. Tsunami simulations for the incipient slope failure and its future slide to completion: For each scenario, wave propagation shown at T = 1:30, 2:50, and 4:20 and color scale depicts max wave heights at the coast. (a–c), Simulates the incipient slope failure which yields a peak wave height of 10 m in Mousa Bay (Egypt) and at 11 m on the Saudi coastline of Tiran Island. Simulated next is the incipient failure sliding to completion with a depth to the basal surface of the slide set to 50 m (d–f) and the less conservative case of 100 m (g–i). Wave heights peak in Mousa Bay at 30 m for the 50 m-thick slide and 45 m for the 100 m-thick slide. In both cases, the impact of the wave is concentrated on the waterfront of Sharm El Sheikh by T = 1:30. *Red line* in (d–i) denotes position of the coastline prior to inundation. The wave inundates >1 km inland at Sharm El Sheikh by T = 2:50. The wave generated by the full slide reaches the Saudi coastline by T = 4:20, with peak heights exceeding 10 m for basal depths of both 50 and 100 m. Animations as Suporting Information S1.

20 seconds of sliding holds disproportionate sway over wave size. During this time, the slide has only moved 1/5th of the way down slope, but the wavefront already traveled halfway across the Straits. This behavior explains why even the incipient slide had a substantial impact on the Egyptian coastline (Figures 5a–5c).

With radiometric dating pinning scarp formation within the last 500 years, it is curious that a 10 m-high tsunami escaped note in the historical record. It cannot be due to wave size, even the largest earthquakes on Earth rarely generate tsunami 10-m high. More likely, the tsunami went unnoticed because it was not associated with an

earthquake. Also relevant is the typically limited spatial extent of landslide tsunami, which emanate from a small point source, versus earthquake tsunami, which radiate from long rupture lines. In this way, the largest quakes on Earth suffer coastlines with inundations over hundreds or thousands of kilometers. Since the Tiran Straits are so narrow, the landslide waves in this study inflicted coastlines spanning just tens of kilometers (Figure 5). Even the main population center today, Sharm El Sheikh, where the brunt of the tsunami inundated the coastline, was little more than an occasional base of operations for local fishermen prior to the 1970s. In antiquity, the settlement of Sharm was situated right at the southern end of the modern city, outside the Straits, and therefore not in the most impacted area. Hence, the lack of a historical record is understandable. We anticipate that geological evidence on land has also been erased by the construction of the modern city of Sharm, though it should be pursued with coring.

We recognize that the incipient slide which we have discovered in the Tiran Straits is only one component of the overall tsunami hazard in the region. Movement of the normal faults bounding the three deep basins that form the Gulf of Aqaba is well poised to be tsunamigenic (Ben-Avraham et al., 1979; Salamon et al., 2021), as is the slip of any of the faults that comprise the DST system (Frucht et al., 2019). Neither are steep submarine slopes restricted to the east side of the Straits. The slopes offshore Sharm El Sheikh, for instance, are equally steep (Figure 1b) and doubtless also at risk of failure, thereby posing an equivalent hazard to the Saudi coast of the Gulf of Aqaba as we simulate for the Egyptian coast.

Ultimately, our model suggests that even incipient landslides, like the one we discovered, can spawn tsunami as tall as those from $M_w = 9$ earthquakes, at least locally. Incipient failures also carry the dual threat of eventually sliding to completion, yielding still larger tsunami sometime in the future.

3.5. Uncertainty and Limitations

Our simulations predict that a complete margin collapse along the full breadth of the scarp has the potential to yield a catastrophic tsunami. With all else fixed, simulations confirm that wave size is more-or-less proportional to landslide thickness. Herein lies one uncertainty. First, the depth to the basal surface of the slide (which dictates its thickness) cannot be known without coring or seismic imaging. We select basal surface depths of 50 m as the moderate case and 100 m as the worst case. Both selections see substantial waves impact Egypt and Saudi. Halving the landslide thickness decreases wave heights at the coast by approximately one third. Therefore, the hazard uncertainty posed by shallower or deeper selections of basal surface depth can be appraised. Depth to basal surface would have to be set to 400 m to deliver a margin scallop equivalent to that of the complete failure that has already occurred immediately to the north (Figure 2b). Though within the realm of possibility, we deem a slide of such extreme magnitude unlikely for a single event.

A second unknown is the depth downslope to where the margin will fail. Based on the extent of the two older failures to the north of our scarp, we set this depth to be 650 m (Figure 2b), but this could be shallower or deeper (the toe-of-slope is at 850 m water depth and bounded by the Tiran fault). Our analysis suggests the 6-km-long scarp formed quickly in one episode. The simulations extrapolated this information to the full failure case by letting the slope fail simultaneously and completely along the entirety of the scarp. Such a comprehensive failure is not guaranteed. Reduction in landslide width translates to a reduction in volume and a smaller and narrower zone of tsunami impact. Framed by these uncertainties, while we consider the range of simulations presented as credible, alternative paths exist in the way a future collapse might proceed, each with different tsunamigenic potential.

3.6. The Risk Is High When the Rift Is Narrow

Reef slopes often collapse, as attested to by the ubiquitous failure scars that adorn the flanks of carbonate shelves and platforms globally, for example, Schnyder et al. (2016). The high propensity for failure stems directly from the fact that carbonate-depositional environments build steep slopes rapidly (Kenter, 1990; Schlager & Camber, 1986). Aggrading swiftly, these slopes tend to be poorly cemented and prone to gravitational instability. This tendency is further amplified by diagenetic heterogeneity wrought by high-amplitude glacial sea-level oscillations. Hence, on geological timescales, slope failures of sufficient magnitude to generate tsunami are common. Given that landslide tsunami radiate most strongly downslope, away from shore, their hazard is somewhat diminished by the long distances that the wave usually travels prior to impacting a coastline. The Bahamian carbonate platforms provide a case in point (Schnyder et al., 2016). A 9-km-wide submarine landslide on western Great

Bahama Bank generates an initial wave height of 6.2 m, but this diminishes to 1.5 m by the time it reaches Florida 100 km away. By contrast, tsunami hazard is amplified in rift basins for several reasons. First, if situated in the reef belt, carbonates accumulate prodigiously and precariously on the rift margins (Purkis et al., 2010, 2012). Second, deep rift basins develop exceptionally steep slopes (>30° in this area, Figure 2b). Third, rifts are tectonically active. Strong earthquakes can trigger slope failures. Finally, rift basins are narrow. Once a tsunami starts, it has little opportunity to attenuate before impacting the opposite coast (Goodman Tchernov et al., 2016). This last fact makes the present case so worrying. The urban center of Sharm El Sheikh is situated only 4.5 km from the anticipated point of slope failure on the opposite side of the Gulf. Arriving at Sharm in just over 1 min, such a wave event would leave little option for early warning. Whereas, earthquake shaking might be construed as a warning, there is no guarantee that slope failure will not be triggered by gravity alone.

4. Conclusions

Rapid urbanization of the Egyptian and Saudi Arabian coastlines of the Gulf of Aqaba necessitates recognition of the tsunami hazard presented by slope failures in the Tiran Straits. We have identified an area with potential for downslope failure in the Straits which would result in a potentially devastating tsunami should it slide to completion. Our model predicts that the incipient (stalled) slide would have generated a tsunami with wave heights up to 10 m at the coast, while a complete slide has the potential to yield waves more than double that height. The steep margins of the Straits are inherently unstable due to the combination of pervasive seismicity and aseismic tectonic activity, coupled with ongoing sediment accumulation from flashfloods and the breakdown of coral reefs. Tsunamis generated from these slope failures will make landfall quickly, with little time for evacuation or response; making efforts to raise awareness and establish coastal management and disaster plans for purposes of mitigating loss-of-life a high priority.

Conflict of Interest

The authors declare no conflicts of interest relevant to this study.

Data Availability Statement

The multibeam data used to achieve this study are available online: https://zenodo.org/record/5781603#.YfI-P2OrMKUl (DOI: https://doi.org/10.5281/zenodo.5781603).

Acknowledgments
The authors owe a debt of gratitude to our Saudi Arabian partners, Neom, and to Paul Marshall, in particular, for facilitating the Deep Blue expedition. They are similarly indebted to the OceanXplorer crew, through the generosity of Mark Dalio, for their inexhaustible help in the field. Special thanks go to Colleen Peters for her commitment to acquiring excellent multibeam, to Andrew Craig and his crew for seamless ROV ops, and to Buck Taylor and his exceptional team of submersible pilots who safely collected samples despite high seas, strong currents, and demanding scientists. The authors are grateful to Simon Day for his advice on bracketing the timing of the slide and to two anonymous reviewers for their insightful critique. G. Chimienti was supported by the Italian Ministry of Education, University and Research (PON 2014–2020, Grant AIM 1807508-1, Linea 1).

References

Abdel-Fattah, A. K., Hussein, H. M., Ibrahim, E. M., & El Atta, A. A. (1997). Fault plane solutions of the 1993 and 1995 Gulf of Aqaba earthquakes and their tectonic implications. *Annals of Geophysics*, *40*, 1555–1564. https://doi.org/10.4401/ag-3831

Augustin, N., Van der Zwan, F. M., Devey, C. W., & Brandsdóttir, B. (2021). 13 million years of seafloor spreading throughout the Red Sea basin. *Nature Communications*, *12*(1), 1–10. https://doi.org/10.1038/s41467-021-22586-2

Baer, G., Sandwell, D., Williams, S., Bock, Y., & Shamir, G. (1999). Coseismic deformation associated with the November 1995, M_w = 7.1 Nuweiba earthquake, Gulf of Elat (Aqaba), detected by synthetic aperture radar interferometry. *Journal of Geophysical Research*, *104*(B11), 25221–25232. https://doi.org/10.1029/1999jb900216

Ben-Avraham, Z. (1985). Structural framework of the Gulf of Elat (Aqaba), northern Red Sea. *Journal of Geophysical Research*, *90*, 703–726. https://doi.org/10.1029/jb090ib01p00703

Ben-Avraham, Z., Almagor, G., & Garfunkel, Z. (1979). Sediments and structure of the Gulf of Elat (Aqaba)-northern Red Sea. *Sedimentary Geology*, *23*, 239–267. https://doi.org/10.1016/0037-0738(79)90016-2

Ben-Menahem, A. (1991). Four thousand years of seismicity along the Dead Sea rift. *Journal of Geophysical Research*, *96*(B12), 20195–20216.

Bosworth, W., Montagna, P., Pons-Branchu, E., Rasul, N., & Taviani, M. (2017). Seismic hazards implications of uplifted Pleistocene coral terraces in the Gulf of Aqaba. *Scientific Reports*, *7*(1), 1–13. https://doi.org/10.1038/s41598-017-00074-2

Frucht, E., Salamon, A., Gal, E., Ginat, H., Grigorovitch, M., Shem Tov, R., & Ward, S. (2019). A fresh view of the tsunami generated by the Dead Sea transform, 1995 M_w 7.2 Nuweiba earthquake, along the Gulf of Elat-Aqaba. *Seismological Research Letters*, *90*(4), 1483–1493.

Garfunkel, Z. (2014). Lateral motion and deformation along the Dead Sea transform. In *Dead sea transform fault system: Reviews* (pp. 109–150). Springer. https://doi.org/10.1007/978-94-017-8872-4_5

Goldberg, M., & Beyth, M. (1991). Tiran Island: An internal block at the junction of the Red Sea rift and Dead Sea transform. *Tectonophysics*, *198*(2–4), 261–273. https://doi.org/10.1016/0040-1951(91)90154-k

Goodman Tchernov, B., Katz, T., Shaked, Y., Qupty, N., Kanari, M., Niemi, T., & Agnon, A. (2016). Offshore evidence for an undocumented tsunami event in the 'low risk' Gulf of Aqaba-Eilat, Northern Red Sea. *PLoS One*, *11*(1), e0145802. https://doi.org/10.1371/journal.pone.0145802

Kahng, S. E., Akkaynak, D., Shlesinger, T., Hochberg, E. J., Wiedenmann, J., Tamir, R., & Tchernov, D. (2019). Light, temperature, photosynthesis, heterotrophy, and the lower depth limits of mesophotic coral ecosystems. In *Mesophotic coral ecosystems* (pp. 801–828). Springer. https://doi.org/10.1007/978-3-319-92735-0_42

Katz, T., Ginat, H., Eyal, G., Steiner, Z., Braun, Y., Shalev, S., & Goodman-Tchernov, B. N. (2015). Desert flash floods form hyperpycnal flows in the coral-rich Gulf of Aqaba, Red Sea. *Earth and Planetary Science Letters*, *417*, 87–98. https://doi.org/10.1016/j.epsl.2015.02.025

Kenter, J. A. (1990). Carbonate platform flanks: Slope angle and sediment fabric. *Sedimentology*, *37*(5), 777–794. https://doi.org/10.1111/j.1365-3091.1990.tb01825.x

Klinger, Y., Rivera, L., Haessler, H., & Maurin, J. C. (1999). Active faulting in the Gulf of Aqaba: New knowledge from the M_w 7.3 earthquake of 22 November 1995. *Bulletin of the Seismological Society of America*, *89*(4), 1025–1036. https://doi.org/10.1785/bssa0890041025

Mart, Y., Hall, J. K., & Vachtman, D. (2018). Tiran Straits: The transfer zone between the Red Sea and the Gulf of Elat and its tectonic significance. *Marine and Petroleum Geology*, *97*, 105–112. https://doi.org/10.1016/j.marpetgeo.2018.06.028

Purkis, S. J., Harris, P. M., & Ellis, J. (2012). Patterns of sedimentation in the contemporary Red Sea as an analog for ancient carbonates in rift settings. *Journal of Sedimentary Research*, *82*(11), 859–870. https://doi.org/10.2110/jsr.2012.77

Purkis, S. J., Rowlands, G. P., Riegl, B. M., & Renaud, P. G. (2010). The paradox of tropical karst morphology in the coral reefs of the arid Middle East. *Geology*, *38*(3), 227–230. https://doi.org/10.1130/g30710.1

Ribot, M., Klinger, Y., Jónsson, S., Avsar, U., Pons-Branchu, E., Matrau, R., & Mallon, F. L. (2021). Active faults' geometry in the Gulf of Aqaba, southern Dead Sea Fault, illuminated by multibeam bathymetric data. *Tectonics*, *40*(4), e2020TC006443. https://doi.org/10.1029/2020tc006443

Salamon, A., Frucht, E., Ward, S. N., Gal, E., Grigorovitch, M., Shem-Tov, R., et al. (2021). Tsunami hazard evaluation for the head of the Gulf of Elat-Aqaba, northeastern Red Sea. *Frontiers of Earth Science*, *8*, 712. https://doi.org/10.3389/feart.2020.602462

Salem, E. S. M. (2009). Paleo-tsunami deposits on the Red Sea beach, Egypt. *Arabian Journal of Geosciences*, *2*(2), 185–197. https://doi.org/10.1007/s12517-008-0027-8

Schlager, W., & Camber, O. (1986). Submarine slope angles, drowning unconformities, and self-erosion of limestone escarpments. *Geology*, *14*(9), 762–765. https://doi.org/10.1130/0091-7613(1986)14<762:ssadua>2.0.co;2

Schnyder, J. S., Eberli, G. P., Kirby, J. T., Shi, F., Tehranirad, B., Mulder, T., et al. (2016). Tsunamis caused by submarine slope failures along western Great Bahama Bank. *Scientific Reports*, *6*(1), 1–9. https://doi.org/10.1038/srep35925

Shaked, Y., Agnon, A., Lazar, B., Marco, S., Avner, U., & Stein, M. (2004). Large earthquakes kill coral reefs at the north-west Gulf of Aqaba. *Terra Nova*, *16*(3), 133–138. https://doi.org/10.1111/j.1365-3121.2004.00541.x

Sun, Q., & Leslie, S. (2020). Tsunamigenic potential of an incipient submarine slope failure in the northern South China Sea. *Marine and Petroleum Geology*, *112*, 104111. https://doi.org/10.1016/j.marpetgeo.2019.104111

Thingbaijam, K. K. S., Martin Mai, P., & Goda, K. (2017). New empirical earthquake source-scaling laws. *Bulletin of the Seismological Society of America*, *107*(5), 2225–2246. https://doi.org/10.1785/0120170017

Tibor, G., Niemi, T. M., Ben-Avraham, Z., Al-Zoubi, A., Sade, R. A., Hall, J. K., et al. (2010). Active tectonic morphology and submarine deformation of the northern Gulf of Eilat/Aqaba from analyses of multibeam data. *Geo-Marine Letters*, *30*(6), 561–573. https://doi.org/10.1007/s00367-010-0194-y

Wang, J., Ward, S. N., & Xiao, L. (2015). Numerical modelling of rapid, flow-like landslides across 3-D terrains: A tsunami squares approach to El Picacho landslide, El Salvador, September 19, 1982. *Geophysical Journal International*, *201*(3), 1534–1544. https://doi.org/10.1093/gji/ggv095

Wang, J., Ward, S. N., & Xiao, L. (2019). Tsunami squares modelling of the 2015 June 24 Hongyanzi landslide generated river tsunami in three Gorges Reservoir, China. *Geophysical Journal International*, *216*(1), 287–295. https://doi.org/10.1093/gji/ggy425

Wawrzyniec, T. F., Selverstone, J., & Axen, G. J. (2001). Styles of footwall uplift along the Simplon and Brenner normal fault systems, central and Eastern Alps. *Tectonics*, *20*(5), 748–770. https://doi.org/10.1029/2000tc001253

Xiao, L., Ward, S. N., & Wang, J. (2015). Tsunami squares approach to landslide-generated waves: Application to Gongjiafang landslide, three Gorges Reservoir, China. *Pure and Applied Geophysics*, *172*(12), 3639–3654. https://doi.org/10.1007/s00024-015-1045-6

Yielding, G., & Roberts, A. (1992). *Footwall uplift during normal faulting: Implications for structural geometries in the North Sea, Structural and tectonic modelling and its application to petroleum geology* (pp. 289–304). Elsevier. https://doi.org/10.1016/b978-0-444-88607-1.50025-5

References From the Supporting Information

Chimienti, G. (2020). Vulnerable forests of the pink sea fan *Eunicella verrucosa* in the Mediterranean Sea. *Diversity*, *12*(5), 176. https://doi.org/10.3390/d12050176

Chimienti, G., De Padova, D., Mossa, M., & Mastrototaro, F. (2020). A mesophotic black coral forest in the Adriatic Sea. *Scientific Reports*, *10*(1), 1–15. https://doi.org/10.1038/s41598-020-65266-9

Eberli, G. P., & Betzler, C. (2019). Characteristics of modern carbonate contourite drifts. *Sedimentology*, *66*(4), 1163–1191. https://doi.org/10.1111/sed.12584

Heaton, T. J., Köhler, P., Butzin, M., Bard, E., Reimer, R. W., Austin, W. E., et al. (2020). Marine20: The marine radiocarbon age calibration curve (0–55,000 cal BP). *Radiocarbon*, *62*(4), 779–820. https://doi.org/10.1017/rdc.2020.68

Niemann, H., Richter, C., Jonkers, H. M., & Badran, M. I. (2004). Red Sea gravity currents cascade near-reef phytoplankton to the twilight zone. *Marine Ecology Progress Series*, *269*, 91–99. https://doi.org/10.3354/meps269091

Reimer, P. J., & Reimer, R. W. (2001). A marine reservoir correction database and on-line interface. *Radiocarbon*, *43*(2A), 461–463. https://doi.org/10.1017/s0033822200038339

Schnyder, J. S., Eberli, G. P., Betzler, C., Wunsch, M., Lindhorst, S., Schiebel, L., et al. (2018). Morphometric analysis of plunge pools and sediment wave fields along western Great Bahama Bank. *Marine Geology*, *397*, 15–28. https://doi.org/10.1016/j.margeo.2017.11.020

Stuiver, M., Reimer, P. J., & Reimer, R. W. (2021). *CALIB 8.2*. Retrieved from http://calib.org